

# Measuring Cosmological Redshift

## Andras Hidas

### **ABSTRACT**

Measuring cosmological redshifts is critical to the study of cosmology. This project demonstrates that equipment is now available to serious amateurs for spectroscopy including the measuring of cosmological redshifts of the brighter quasars. The redshift of magnitude 12.8V quasar 3C273 in Virgo and magnitude 13.8V quasar HE 1029-1401 in Hydra was successfully measured as 0.157 (+/-0.003) and 0.081 (+/-0.003). These results are 0.6% and 5.2% in error with respect to the accepted values. The first figure is within the estimated error range. The reason for the larger error for the second object appears to be an unexplained systematic error.

### **1. INTRODUCTION**

The Standard Cosmological Model of the universe holds that the universe began about 13.8Gyr ago and expanded from a singularity, a theory known colloquially as the Big Bang. The foundations of the Standard Cosmological Model sometimes called the  $\Lambda$ CDM (Lambda-Cold Dark Matter) model rests on the parameters  $H_0$  the Hubble constant and  $\rho_0$  the matter/energy density. The subscripts stand for current values.

$H_0$ , generally accepted range of values 50 . 80-  $\text{kms}^{-1}\text{Mpc}^{-1}$ (SAOweb1), sets the distance and time scale of the universe. A great deal of observational cosmology is devoted to nailing it down to an accurate value. The main tool for researching the Hubble constant is the measurement of cosmological redshift of galaxies. In practice the value accepted by most astronomers is that found by the WMAP CMB (Cosmic Microwave Background) survey of 70 (+/-2.2)  $\text{kms}^{-1}\text{Mpc}^{-1}$  (NASAweb1)

Cosmological redshift is to be distinguished from conventional Doppler shift where light (or sound) emitted from a radially moving source is seen by an observer to increase in wavelength when receding (redshifted) or decrease in wavelength (blueshifted) when approaching. Cosmological redshift, while similarly caused by relative velocity between the source and observer, is not caused by actual movement of source and observer but by the cosmological expansion of space as required by the Big Bang theory. Normal heliocentric Doppler shifts of stars and galaxies can be redshifts or blueshifts. Cosmological redshifts are said to be observed at more than  $z=0.01$  (about  $3000\text{kms}^{-1}$  at the distance of about 40Mpc) (SAOweb1), where galaxies are part of the Hubble Flow. (Tonry 1981) This definition is a little arbitrary because the random motion of galaxies in the local universe swamps the magnitude of the cosmological redshifts at small distances.

Cosmological redshift  $z$  is defined in Hubble's Law (Ryden 2003)

$$v(d) = H_0 d = cz$$

Where:

$v(d)$   $\text{kms}^{-1}$  recession velocity (function of distance),  
 $c$   $\text{kms}^{-1}$  speed of light,  
 $z$  redshift,  
 $d$  Mpc (megaparsecs) distance  
 $H_0$   $\text{kms}^{-1}\text{Mpc}^{-1}$  Hubble constant

The redshift of an object is determined by observing its spectrum. If a spectral feature, for which the rest wavelength is known, can be identified the redshift  $z$  can be calculated.

$$z = \left( \frac{\lambda_{\text{obs}}}{\lambda_{\text{em}}} \right) - 1$$

Where

$\lambda_{\text{obs}}$  measured wavelength  
 $\lambda_{\text{em}}$  emitted (rest) wavelength

Spectral features can be either emission or absorption lines. For small values of  $z$  the Balmer series, mainly H $\alpha$ , H $\beta$  and H $\gamma$  are used. At higher redshifts the Lyman series are shifted into the visible spectrum and can be used with conventional detectors. At the extreme end of redshift measurement, currently around  $z=7$ , conventional spectrographs cannot be used due to the extreme faintness of remote galaxies, photometric spectroscopy is used. Photometric spectroscopy uses a series of filters to detect spectral features such as the Lyman break.

Quasars (or QSOs) are the most energetic of a class of objects generally referred to as Active Galactic Nuclei (AGN). AGN are cores of galaxies containing a Supermassive Black Holes (SMBH) at their centres. They appear as a variety of high luminosity objects with their active accretion discs at different angles to our line of sight with some cores hidden behind dust tori. Most QSOs are at cosmological distances with redshifts well into the Hubble Flow. The first QSO was identified by Alan Sandage as the source of energetic radio emissions but it was Marteen Schmidt (Greenstein & Schmidt 1964) who first realised that the strange spectrum of 3C273 was due to a large redshift of its Balmer hydrogen emission lines. Schmidt then realised that 3C273 was at a cosmological distance of 480Mpc. Since then, thousands of QSOs have been discovered at distances up to  $z=7.085$  (Mortlock 2011) and they have become essential tools in probing the universe at cosmological distances.

Due to their extraordinary luminosity, a few of the brighter QSOs, including 3C273, are within reach of modest amateur telescopes despite their cosmological distances.

The objective of this project was to measure the redshift of two readily accessible quasars using an amateur telescope and an inexpensive diffraction grating and associated spectrum analysis software. It was also aimed to explore, estimate and minimise the sources of error.

The objects chosen for this project were QSOs

3C273 . in Virgo, the closest and brightest quasar at 12.9V  
 HE 1029-1401 . in Hydra a quasar of magnitude 13.8V

## 2. EQUIPMENT

The redshift of an object, a star or a galaxy, is determined by measuring the displacement of well known spectral features using a spectrometer attached to a telescope. The equipment available for this project is part of Arcadia Observatory, a small private amateur observatory dedicated to newly discovered Near Earth Object (NEO) follow up astrometry. The observatory is located a little north of metropolitan Sydney in rural residential surroundings with reasonably dark skies. The following equipment was used on the redshift project:

- Celestron C14 (14+(350mm) f11) Schmidt-Cassagrain Telescope (SCT). The original model had a basic synchronous motor drive in RA (solar rate), small DC motors as manual drive correctors and mechanical setting circles. The telescope is now equipped with computer controlled custom made drive electronics using *Argo Navis* high resolution digital setting circles made by Wildcard Innovations. The telescope is remotely operable with semi GOTO capability over a private Local Area Network (LAN) from the on site residence.
- Sky Watcher 150mm Newtonian guide scope mounted on the C14 and equipped with an SBIG SG4 standalone autoguider camera capable on guiding on a magnitude 11 star with  $<1\mu$  error
- SBIG ST8300M TEC cooled CCD camera. Kodak KAF8300 CCD chip, 6Mpix, pixel size  $5.4\mu\text{m}$ , 2x2, 3x3 binnig capability.
- Lumicon *Giant Easy-Guider* focal reducer for wide angle (FOV  $25\alpha 19\alpha$ ) imaging. Effective focal ratio and focal length of C14 reduced to  $\sim f/7$  and 2520mm.
- Diffraction grating made by Paton Hawksley, Star Analyser 100 (SA100). This is a 100 lines/mm blazed transmission grating purchased for the project at a reasonable price

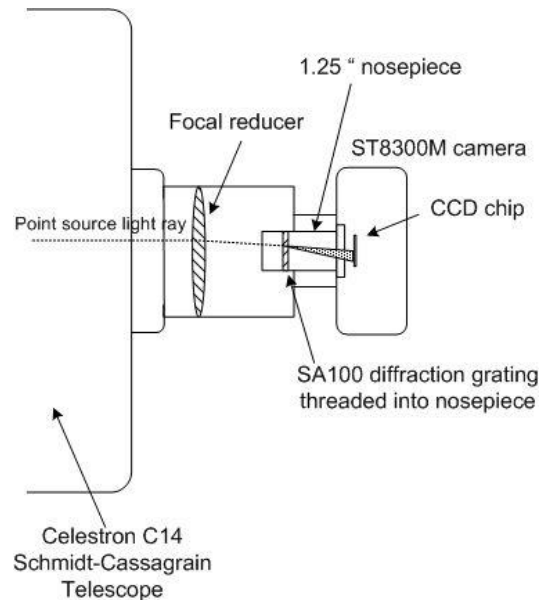


Fig 1. SA100 diffraction grating

For spectroscopy the diffraction grating is screwed into the front of a 1.25+ camera adaptor nosepiece. Figure 2 shows the arrangement of grating and camera set up for spectroscopy.



Photograph of observatory equipment.



Simplified optical schematic of spectrograph  
 Fig 2 Arrangement for spectroscopy

The optical configuration shown in Figure 2. constitutes a slitless spectrograph. A slit is not required as the objects being observed are point sources. (including the QSOs). The blazed transmission grating is placed in the path of light near the detector (CCD chip) and the image of stars in the field of view are dispersed (smeared) forming elongated images constituting the spectrum of component wavelengths of the source. The angle of dispersion is given by the *grating equation*  $m = \sin \theta_i + \sin \theta_d$  where  $m$  is the order number ( $m=1$  in practice for blazed grating),  $\lambda$  is wavelength,  $g$  is groove pitch (0.01mm),  $\theta_i$  is angle of incidence. (Birney 2006).

The distance of the grating from the CCD chip depends on the desired spectral resolution on the CCD chip (Angstroms/pixel):

$D = 10,000 \cdot s_{pix} / g \cdot d$   $D$  is dispersion (Angstroms/pixel),  $s_{pix}$  is pixel size in microns,  $g$  is grating lines/mm,  $d$  is distance of grating from CCD chip in mm.  
 (Paton Hawksley Education SA100 User Manual v1.6)

In Figure 2,  $d$  is 71mm, giving 15.1 Angstroms/pixel resolution on the CCD chip using 10.8 micron pixels (2x2 binning). Binning is required to achieve acceptable image SNR for reasonable exposure. 2x2 binning was used on 3C273 to maximise spectral resolution. 3x3 binning was used on HE 1029-1401 to maintain acceptable SNR.

The following suite of software was used for in this project:

- *CCDops* camera control software . from camera manufacturer SBIG
- *Astrometrica* -- Astrometry software by Herbert Raab
- *RSpec* - Spectrum analyser software from Paton Hawksley Education
- *Guide 7* Planetarium software by Bill Gray from Project Pluto

### 3. OBSERVING THE QUASARS

The selection of targets for this project was constrained by a number of immutable factors: timeframe set by the 12 week semester, capability of available equipment and observability of potential targets in the semester timeframe (2/3/15 to 23/5/15) from the observing site. With a stroke of luck, the prime target, the brightest quasar, 3C273 was visible after 10 pm from Sydney during the whole semester. Facing a steep learning curve involving spectroscopy, test observations of 3C273 were made very early in the project. It was clear during the first observing session (using the newly acquired diffraction grating) that obtaining useful spectrum of 3C273 is not going to be a problem. A trial version of RSpec spectrum analyser software confirmed that usable spectrum was recorded even with short stacked images during the first observing session. The second target quasar was a lot harder to select. Using a list of bright quasars and other AGN objects (SpaceteWeb) containing over 400 entries, there was only one object other than 3C273 that is brighter than 15V in the southern hemisphere sky. QSO HE 1029-1401 is one of the brightest quasars in the sky and the first to be discovered by visual wavelengths, by Wisotzki (1991). It is listed at 13.9V a full magnitude fainter than 3C273.

A number of issues needed to be resolved before settling on the final configuration:

*Exposure time.* At magnitude 12.8V 3C273 appears to be an easy target for observing with a 14 inch (350mm) telescope. However we are not observing the flux of the object concentrated into a tiny aperture circle (typically 5 pixels for astrometry) the image (and total flux) of the spectrum of the object is spread out over hundreds of pixels. The result is that the flux per pixel is 5 to 6 magnitudes fainter than direct observation. (Field 2015). The C14 used in this project normally reaches to about 19V for astrometry, so a magnitude 13V quasar is close to its limit for spectroscopy. Eventually 15 minute exposures were found to be satisfactory for this object. Good guiding is an unavoidable requirement. In addition there are no bright guide stars in the immediate vicinity. To reach the second target QSO, HE 1029-1401, with similar exposure time 3x3 binning was necessary, compromising the spectral resolution with the larger pixels.

*Grating spacing.* The placement of the grating from the CCD chip is a trade off between sufficient spectral resolution and image length to fit on the chip. Also if the spectrum is spread too much the image is fainter and longer exposure is required. Spatial restrictions in the way the camera is attached to the telescope is another constraint. The SA100 grating is designed to fit into filter threading in 1.25 inch eyepieces or camera adaptors. To get the optimum spacing, extra adaptor or spacers may be required. On the C14 used in this project an extra long 2 inch T thread camera adaptor with a 1.25 inch converter was used to achieve the target spectral resolution of 10 to 20 Angstroms/pixel on the chip. At 71mm from the chip with 10.8 micron pixels (2x2 binning) 15.1 Angstrom/pixel is achieved.

*Grating line orientation.* For a specific target in the field being imaged, the grating must be oriented (rotated) in such a way that the image of its spectrum does not fall on other stars zero order image or the image of another star's spectrum.

*Calibration.* Initially RSpec converts the monochrome FITS image of the spectrum to graphical representation, plotting relative intensity values (y axis) against pixel positions (x axis). To be useful the x axis must be converted to Angstroms using the correct scale factor (dispersion, angstroms/pixel) and 0 offset. This is done by using a star for which the

spectral features are known and have no significant radial motion. A spectral type A0 star is recommended as it has prominent Balmer hydrogen lines with well known wavelengths. Calibration to obtain the correct scale factor is done by setting the zero point on the zero order peak then selecting one of the more obvious Balmer lines, usually the H $\gamma$  line and setting it to its known wavelength of 4861.3 Å. RSpec then calculates the dispersion scale factor  $D = 4861.3 / (\text{Pixel}_H - \text{Pixel}_{0\text{-order}})$ . This of course assumes a perfectly linear grating. This calibration is only valid for the particular position (distance from the chip) of the grating. RSpec recommends using Vega as calibration star, however Vega is on the wrong hemisphere and obvious type A stars were hard to find in the accessible sky. Eventually a magnitude 10V star in the field of QSO 3C273, star PPM158889, had identifiable H $\gamma$  and H $\beta$  absorption lines. This had the added advantage that calibration images required no separate exposures. During calibration measurements it was found that using the H $\gamma$  line to set the scale, the H $\beta$  line would be consistently misaligned by a minor but consistent amount of 2 to 3 pixels. This was evidence of minor non-linearity in the grating. The calibration function in the software handles this possibility by providing a non-linear calibration alternative where a selectable order polynomial is fitted to multiple lines in the calibration star's spectrum. With this process all known lines can be made to fit the selected template.

Setting up and testing has taken 6 observing sessions between 27/2/2015 and 15/3/2015. The final production run for accurate data for the two objects was done over 2 nights with the collection of 11 images for each object. All exposures were of 15 minute duration. Table 1 lists object details.

Name	Co-ordinates	Magnitude V	Images recorded	Exposure time	Binning	Image size
3C273	RA 12h29m07s Dec +02°03'08"	12.8	11	15 min	2x2	1676 x 1266
HE 1029-1401	RA 10h31m54s Dec -14°16'52"	13.9	11	15 min	3x3	1117 x 844

Table 1. Summary of target QSOs

#### 4. DATA REDUCTION

The results of the final two observing sessions are 22 FITS images. The FITS format (Flexible Image Transport System) is the standard generally used in astronomy and is supported by all serious astronomy software.



Fig 3. 3C273 typical one of 11 images

Fig 4. HE1029 typical one of 11 images

The images were taken and pre-processed in small batches under the control of SBIG *CCDops* software, including the taking and subtraction of a dark frame from each image. The quality of the images was checked by loading into *Astrometrica* where the zero order image of the target was examined. The parameters of the fitted Gaussian PSF (SNR, FWHM and RMS of fit) was recorded. On average, the 2x2 binned 3C273 image had SNR  $\sim 60$ , FWHM  $\sim 2.8+$ , RMS  $\sim 0.15+$ . The 3x3 binned HE1029-1401 images had SNR  $\sim 70$ , FWHM  $\sim 4.2+$ , RMS  $\sim 0.06+$ . As expected the larger pixel size used on the HE1029-1401 images roughly compensated for being one magnitude fainter than 3C273 when using the same 15 minute exposure. Each image was interactively processed and analysed in the RSpec application. The image of the spectrum is rotated into a horizontal position and an adjustable thin ( $\sim 20$  pixel) horizontal measuring box is placed over it. (see Figure 5.)

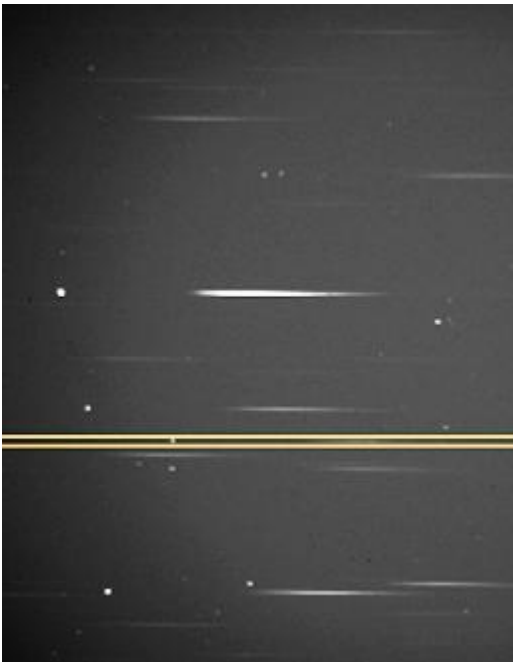


Fig 5. RSpec measuring box

The box is made as small as possible without excluding any of the target flux. The resulting profile includes the zero order and dispersed image of the target and background sky. The raw profile is dominated by the sky background flux in the 15 minute exposures but is easily removed by the software leaving the genuine flux signal and instrument noise.

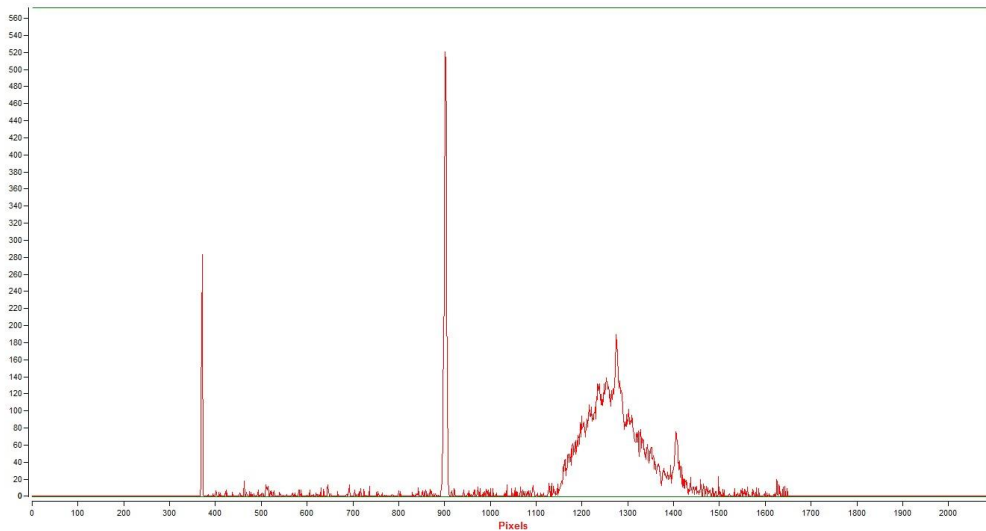
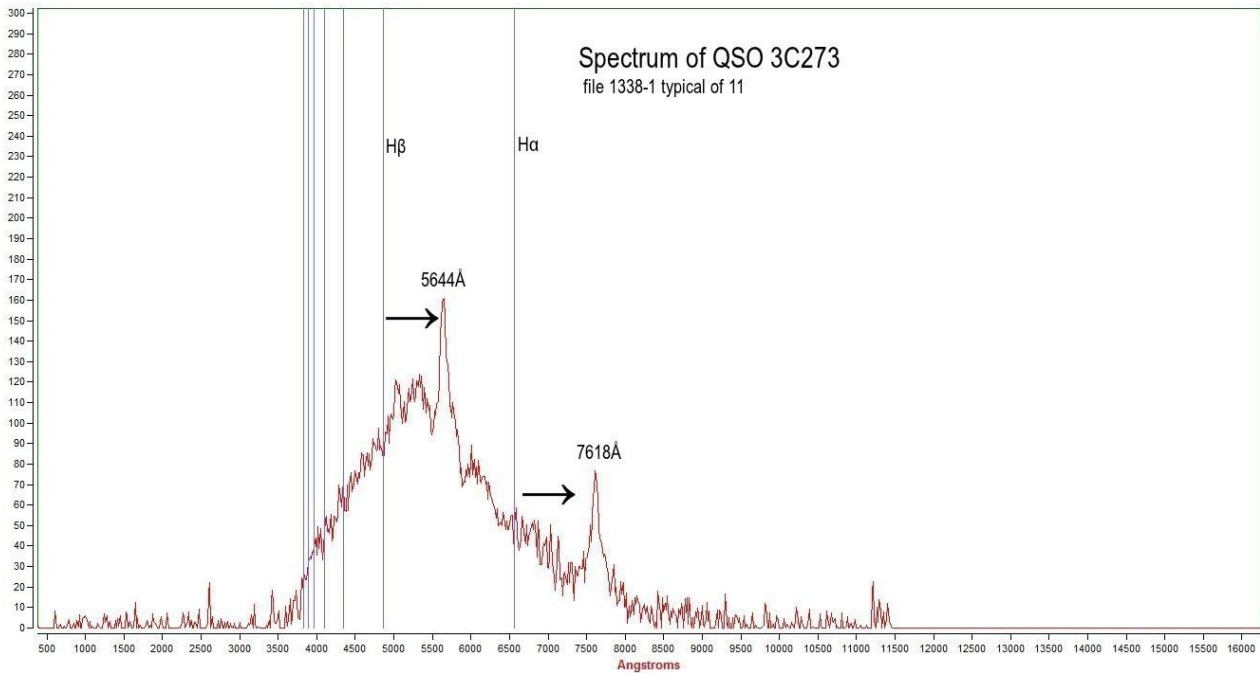


Fig 6. Raw spectrum profile after removal of sky background.

RSPEC plots the spectrum by binning the pixel values vertically across each horizontal pixel position inside the measuring box. See Figure 6 showing the raw spectral profile from the measuring box. The large spike in the middle of the graph is the flux representing the zero order image. The x axis of profile graph is calibrated by setting the zero order spike to zero angstroms and applying the scale factor (dispersion) obtained from the calibration star earlier. The dispersion is 15.1 for the 3C273 images and 22.5 for HE 1029-1401 images. The x axis is then automatically relabelled in angstroms. Fig 7. shows a typical processed spectrum profile. The wavelength of peaks and valleys indicating emission and absorption features in the spectrum respectively can be read off and recorded in RSPEC by the use of narrow vertical parallel *measuring lines* placed around the feature and letting RSPEC compute the barycentre of the enclosed flux.





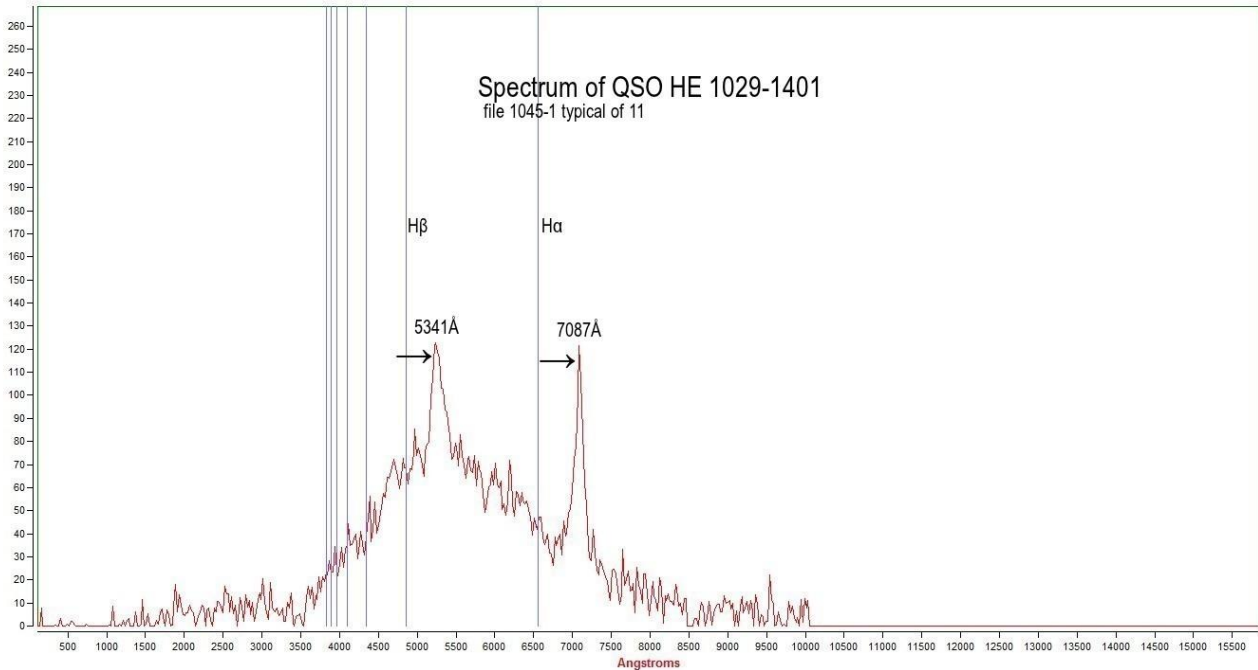


Fig 7. Calibrated spectral profile of 3C273 and HE 1029-1401 showing the displaced spectral features.

There are three main features to be noted that are common to all the QSO spectra taken in this project. (See Figure 7.)

- The continuum flux dominates all profiles with peak relative flux ~110.
- There are two very prominent emission features visible on both 3C273 and HE 1029-1401 which were assumed to be the redshifted Balmer H $\beta$  and H $\alpha$  lines. These peaks are of relative flux height of 50-60 for 3C273 and 60-80 for HE 1029-1401 above the continuum flux.
- Background peak to peak noise consisting of instrument noise and sky background is about 10 on the same scale. This represents about signal to noise ratio (SNR) relative to the target line feature signal of about 6. As we are not interested in the actual flux measurement, only the position of the spectral features, a low SNR is of no concern as far as measuring redshift. It does however mean that weaker spectral features were not obvious as they appeared to be swamped by noise. In Figure 7 the H $\alpha$  line is seen but not quite reliable for measurement as it is only twice as large as the background noise.

All data including the 44 wavelength measures (11 H $\beta$  and H $\alpha$  for each objects) was recorded on an Excel spreadsheet and statistically processed and summarised. Raw pixel data for each wavelength was also recorded so that that verification could be made of RSpec calculations. Assuming a linear dispersion, the wavelength can be calculated from raw pixel data by:  $\lambda = D(p - p_0)$  where  $\lambda$  is the wavelength of the feature being measured, D is scale factor of dispersion, p pixel number of feature (peak or valley),  $p_0$  is pixel number of zero order peak.

Table 2. shows summary of data and results.

Date	file name	Å redshifted H $\alpha$	Published redshifted	Å redshifted H $\beta$	Published redshifted			
<b>3C273</b>								
<b>D=15.1Å/pixel</b>								
19/03/2015	1338-1	7618	7599	5644	5629			
	1338-2	7579		5631				
	1338-3	7607		5649				
	1338-4	7625		5616				
	1338-5	7610		5645				
18/03/2015	1230-1	7584		5620				
	1230-2	7589		5613				
	1230-3	7568		5612				
	1337-1	7569		5615				
	1337-2	7578		5627				
	1337-3	7587		5617				
	<b>mean</b>	<b>7592</b>		<b>5626</b>				
		<b>19.7</b>		<b>13.9</b>				
	Unshifted		6562.8		4861.3			
	<b>redshift Z</b>	<b>0.157</b>	<b>0.158</b>	<b>0.157</b>	<b>0.158</b>			
	<b>mean redshift</b>		<b>0.15711</b>		<b>0.006</b>			
<b>HE 1029-1401</b>								
<b>D=22.5 Å/pixel</b>								
19/03/2015	0939-1	7087	7127.2	5262	5279.4			
	0939-2	7099		5241				
	0939-3	7110		5265				
	1045-1	7087		5341				
	1045-2	7086		5241				
	1045-3	7077		5244				
	1152-1	7087		5261				
	1152-2	7086		5242				
	1152-3	7086		5241				
	1152-4	7106		5245				
	1152-5	7108		5263				
		<b>mean</b>		<b>7092.6</b>			<b>5258.7</b>	
				<b>11.1</b>			<b>29.1</b>	
		Unshifted				6562.8		4861.3
	<b>redshift Z</b>	<b>0.081</b>	<b>0.086</b>	<b>0.082</b>	<b>0.086</b>			
	<b>mean redshift</b>		<b>0.081</b>		<b>0.055</b>			

Table 2. Summary of data and results

## 5. **ERROR ANALYSIS**

The following were identified as sources of error:

- *Quality of image from CCD, image signal to noise ratio.*

All types of CCD astronomy require a good quality image. Assuming the CCD camera use is appropriate for the purpose (adequate resolution, sensitivity, optics) the quality and the suitability of the image for the purpose is usually limited by the signal to noise ratio (SNR) of image data. The main sources of noise (unwanted signal) in CCD imaging is instrumental noise such as dark current, read noise and sky background). The full analysis of CCD SNR is outside the scope of this report but the SNR can always be improved by increasing exposure time. There is a limit however, sky brightness. It was found that for the equipment used in this project, the most important being the focal ratio of the telescope optics (f7/0) the limiting exposure was about 15 minutes before sky brightness saturated the pixels. It was just adequate for the fainter object, resulting in the emission features signal to background noise ratio of about 6. For the purpose of locating spectral peaks this is more than adequate. It is thought that any error due to image SNR had negligible contribution to the final results.

- *Measuring box*

The thickness of the horizontal measuring box placed over the target spectrum image has a large effect on the profile signal to noise ratio. This is because a wide measuring box includes more unwanted signal from sky background and other objects such as faint stars which are included in the vertically binned signal making up the profile. Any noise contribution from this source detracts from the overall SNR of the image. To overcome interfering images from being included in the measuring box, the grating is rotated to clear obvious obstacles. This has to be done for any specific target in a frame. By chance the orientation of the grating suited the images of both targets. The contribution of the residual unwanted flux after orienting the grating is reduced by carefully adjusting the width and position of the measuring box. As this is a manual exercise using the mouse in RSpec, it is very easy to vary the feature SNR (the ratio of line feature height to peak - peak noise) by a factor of 2. Contribution from this error source was considered but eliminated by visually minimising the peak to peak noise while adjusting the measuring box.

- *Grating dispersion*

The effective dispersion scale eventually sets the precision of the wavelength measurement. RSpec recommends dispersion scale of between 10 to 20 Å/pixel. To achieve this range the grating must be placed at a distance from the CCD chip given by  $d = 10,000 s_{\text{pix}} / gD$  Where  $d$  is distance of grating from CCD chip in mm.,  $s_{\text{pix}}$  is pixel size in microns,  $g$  is grating lines/mm,  $D$  is dispersion (Angstroms/pixel) (SA100 User Manual v1.6). Assuming that the position of features on spectrum profile can be read consistently to one pixel the dispersion of 15.1 and 22.5 used in the project sets the higher limit to the accuracy of the result. That is ~ 15 Å for 3C273 and 22 Å for HE 1029-1401

- *Calibration error*

While the previously discussed sources error can be considered to be of the random type, calibration error is of the systematic type. Calibration error applies to all measurements and always in the same direction. Calibration is done by measuring the Balmer hydrogen lines H<sub>β</sub> and H<sub>γ</sub> of a stationary star. For this project a star in the field of the 3C273 target was measured a handful of times in the calibration process of RSpec and displayed and recorded as 15.1 for the 2x2 binned images and 22.5 for the 3x3binned images. The results were consistent to the implied precision of 0.1. The error implied is +/-0.05.

- Error in picking peaks and valley points on the profile.

Selecting the point on the profile in RSpec involves a degree of uncertainty. RSpec estimates the pixel coordinate of a peak or valley to 0.1 pixel precision. It is assumed that this is done by some sort of curve fitting to peak and valley features.. This point on the graph is visually selected and the readout by RSpec has been found to vary by about a pixel either side of the feature. It is estimated that the error involved is approximately +/-1 pixel which translates to +/-15 Å or 22 Å in wavelengths measurement. As each profile measurement needs two peaks to be selected, zero point and feature peak, the total error in reading a wavelength from the profile graph is 1/2 pixels.

- Estimation of total error

The total error in the wavelength measurement in angstroms is estimated by combining the contribution from the two significant error sources, calibration error (dispersion scale D) and selecting profile peaks. Using the expression for the wavelength in terms of pixels and dispersion:  $\lambda = D(p - p_0)$  where D is dispersion scale and p, p<sub>0</sub> are pixel co-ordinates of spectral features and zero order peak respectively, the combined error is given by:

$$\Delta \lambda = (2/p^2 + (D/D)^2)^{1/2}$$

Where  $\Delta \lambda$  is error in wavelength, p is pixel number of wavelength, D is error in dispersion scale factor (~ 0.05). for example for  $\lambda = 7610$  and p = 1410

$\Delta \lambda = (1.0 \times 10^{-6} + 10.1 \times 10^{-6})^{1/2} = 0.0033$  or 0.33%. This translates to  $0.0033 \times 7610 = +25.3$  Å. This is comfortably consistent with the resolution of the grating projected onto the CCD chip.

For the above example the error in redshift ( $z = \lambda / \lambda_0 - 1 = 0.159$ ), is  $\Delta z = \Delta \lambda / \lambda_0$ ,  $\lambda_0$  is 6562.5 the error in z,  $\Delta z = 25.3/6562.8 = 0.0038$

Table 3. shows main results.

Object	Mean Z	Published Z (NED)	Velocity (cz)	Distance = v/H0, H0=70km/s/Mpc
<b>3C273</b>	0.157 (+/-0.003)	0.158	47,100 km/s	673 Mpc
<b>HE 1029-1401</b>	0.081 (+/-0.003)	0.086	24,300 km/s	347 Mpc

Table 3. Final results

## 6. CONCLUSIONS

The results of this attempt at measuring the cosmic expansion of the universe are that the redshift of 3C273 is 0.157 (+/- 0.003) which is  $\sim 0.001$  less than the published figure of 0.158339 (+/- 0.000067) and for HE-1029-1401  $z$  is 0.081 (+/- 0.003) which is about 0.005 less than the published figure of 0.08582 (+/- 0.00009). (NED). While the result for the first and brighter object is pleasing considering the limitations of the equipment, basically the inexpensive diffraction grating the result for HE-1029-1401 is a little disappointing. This should not be surprising as the equipment appeared to be operating close to its limits. The accepted figure for the 3C273 redshift is inside error bars of the measured value in this project. The small offset from the published figure can probably be put down to a systematic error in the calibration. The same dispersion scale was used on all measures whereas there was an opportunity to recalibrate on each image as the calibration star was in the field. The error on the second object is too large and outside the estimated error bars to be explained by a minor calibration error. It is however not entirely surprising as the object was a whole magnitude fainter and the pixel size 50% larger than for 3C273. Regarding the grating nonlinearity issue, the non-linear calibration function of RSpec was not used as the resulting wavelengths had relatively large unexplained offsets. Investigating this issue was abandoned due to the lack of access to the polynomial coefficients used by the program and the eventual lack of time.

## References:

- Birney, D. et al. 2006 Observational Astronomy 2<sup>nd</sup> Ed.  
 Fields, Tom 2015 Private communication  
 Greenstein, J. and Schmidt, M 1964 ApJ 140 1G  
 Mortlock, D. et al. 2011 Nature, vol. 474, p. 616-619  
 NED: <http://ned.ipac.caltech.edu/>  
 NASAweb1: [http://map.gsfc.nasa.gov/universe/uni\\_expansion.html](http://map.gsfc.nasa.gov/universe/uni_expansion.html)  
 Paton Hawksley Education Ltd: Star Analyser 100 User Manual v1.6  
 Ryden, B. 2003 Introduction to Cosmology  
 RSpecWeb1: <http://www.rspec-astro.com/>  
 RSpecWeb2: <http://www.fieldtestedsystems.com/>  
 SAOweb1: Course content (AST80003-M08A02)  
 SIMBAD: <http://simbad.u-strasbg.fr/simbad/>  
 SpaceteWeb: <http://www.klima-luft.de/steinicke/KHQ/anhang.txt>  
 Tonry, J. and Davis, M. 1981 ApJ 216 680T  
 Wisotzki L., Wamsteker W., Reimers D., 1991 A&A 247, L17

## Observation Log

27/2/2015  
 UT 1304            3C372 12 frames 60 sec  
 UT 1339            3C372 25 frames 30 sec

28/2/2015  
 UT 1340            3C372 1 frame 300 sec

UT 1430 3C372 6 frames 240 sec  
UT 1545 3C372 1 frame 600 sec

2/3/2015

UT 0949 PPM 187818 16 frames 8 sec  
UT 0950 PPM 187818 5 frames 16 sec  
UT 1010 PPM 187818 10 frames 4 sec  
UT 1122 PPM 187818 10 frames 8 sec  
UT 1315 3C372 5 frames 600 sec  
UT 1335 3C372 5 frames 120 sec

9/3/2015

Increased grating spacing to improve resolution  
UT 0955 PPM 187818 5 frames 2 sec  
UT 0957 PPM 187818 5 frames 4 sec  
UT 1001 PPM 187818 5 frames 8 sec

14/3/2015

UT 0941 PPM 187818 4 frames 10 sec  
UT 1121 PPM 08402857 4 frames 15 sec

15/3/2015

UT 1357 3C372 2 frames 600 sec  
UT 1434 3C372 3 frames 600 sec

18/3/2015

Changed to 2x2 binning  
UT 1230 3C372 3 frames 900 sec  
UT 1337 3C372 3 frames 900 sec

19/3/2015

3x3 binning for HE-209, 2x2 binning for 3C372  
UT 0939 HE-209 3 frames 900 sec  
UT 1045 HE-209 3 frames 900 sec  
UT 1152 HE-209 5 frames 900 sec  
UT 1338 3C372 5 frames 900 sec